

# Domain wall dynamics in two-dimensional van der Waals ferromagnets


Cite as: Appl. Phys. Rev. **8**, 041411 (2021); <https://doi.org/10.1063/5.0062541>


Submitted: 06 July 2021 • Accepted: 25 October 2021 • Published Online: 29 November 2021

Dina Abdul-Wahab,  Ezio Iacocca,  Richard F. L. Evans, et al.

## COLLECTIONS

Paper published as part of the special topic on [Quantum Materials and 2D superlattices](#)

 This paper was selected as Featured

 This paper was selected as Scilight



View Online



Export Citation



CrossMark

## ARTICLES YOU MAY BE INTERESTED IN

[Recent progress on 2D magnets: Fundamental mechanism, structural design and modification](#)  
Applied Physics Reviews **8**, 031305 (2021); <https://doi.org/10.1063/5.0039979>

[Opportunities in electrically tunable 2D materials beyond graphene: Recent progress and future outlook](#)

Applied Physics Reviews **8**, 041320 (2021); <https://doi.org/10.1063/5.0051394>

[Magnetic field-induced non-trivial electronic topology in  \$\text{Fe}\_{3-x}\text{GeTe}\_2\$](#)

Applied Physics Reviews **8**, 041401 (2021); <https://doi.org/10.1063/5.0052952>



Applied Physics  
Reviews

Read. Cite. Publish. Repeat.

**19.162**  
2020 IMPACT FACTOR\*

# Domain wall dynamics in two-dimensional van der Waals ferromagnets

Cite as: Appl. Phys. Rev. **8**, 041411 (2021); doi: [10.1063/5.0062541](https://doi.org/10.1063/5.0062541)

Submitted: 6 July 2021 · Accepted: 25 October 2021 ·

Published Online: 29 November 2021



View Online



Export Citation



CrossMark

Dina Abdul-Wahab,<sup>1</sup> Ezio Iacocca,<sup>2,3</sup>  Richard F. L. Evans,<sup>4</sup>  Amilcar Bedoya-Pinto,<sup>5</sup>  Stuart Parkin,<sup>5</sup>   
Kostya S. Novoselov,<sup>6,7,8</sup>  and Elton J. C. Santos<sup>9,10,a)</sup> 

## AFFILIATIONS

<sup>1</sup>School of Mathematics and Physics, Queen's University Belfast, Belfast BT7 1NN, United Kingdom

<sup>2</sup>Center for Magnetism and Magnetic Materials, University of Colorado, Colorado Springs, Colorado Springs, Colorado 80918, USA

<sup>3</sup>Department of Mathematics, Physics, and Electrical Engineering, Northumbria University, Newcastle upon Tyne NE1 8ST, United Kingdom

<sup>4</sup>Department of Physics, The University of York, York YO10 5DD, United Kingdom

<sup>5</sup>NISE Department, Max Planck Institute of Microstructure Physics, Halle, Germany

<sup>6</sup>Institute for Functional Intelligent Materials, National University of Singapore, S9, 4 Science Drive 2, 117544, Singapore

<sup>7</sup>Chongqing 2D Materials Institute, Liangjiang New Area, Chongqing 400714, China

<sup>8</sup>National Graphene Institute, The University of Manchester, Oxford Road, Manchester, M13 9PL, United Kingdom

<sup>9</sup>Institute for Condensed Matter Physics and Complex Systems, School of Physics and Astronomy, The University of Edinburgh, Edinburgh EH9 3FD, United Kingdom

<sup>10</sup>Higgs Centre for Theoretical Physics, The University of Edinburgh, Edinburgh EH9 3FD, United Kingdom

**Note:** This paper is part of the special collection on Quantum Materials and 2D superlattices.

**a)** Author to whom correspondence should be addressed: [esantos@ed.ac.uk](mailto:esantos@ed.ac.uk)

## ABSTRACT

Domain wall motion is in the core of many information technologies ranging from storage [Beach *et al.*, J. Magn. Magn. Mater. **320**, 1272–1281 (2008)], processing [Tatara *et al.*, Phys. Rep. **468**, 213–301 (2008)], and sensing [Ralph and Stiles, J. Magn. Magn. Mater. **320**, 1190–1216 (2008)] up to novel racetrack memory architectures [Parkin *et al.*, Science **320**, 190–194 (2008)]. The finding of magnetism in two-dimensional (2D) van der Waals (vdW) materials [Huang *et al.*, Nature **546**, 270 (2017); Gong *et al.*, Nature **546**, 265–269 (2017); Guguchia *et al.*, Sci. Adv. **4**, eaat3672 (2018); Klein *et al.*, Science **360**, 1218–1222 (2018)] has offered a new frontier for the exploration and understanding of domain walls at the limit of few atom-thick layers. However, to use 2D vdW magnets for building spintronics nanodevices such as domain-wall based logic [Allwood *et al.*, Science **309**, 1688–1692 (2005); Luo *et al.*, Nature **579**, 214–218 (2020); Xu *et al.*, Nat. Nanotechnol. **3**, 97–100 (2008)], it is required to gain control of their domain wall dynamics by external driving forces such as spin-polarized currents or magnetic fields, which have so far been elusive. Here, we show that electric currents as well as magnetic fields can efficiently move domain walls in the recently discovered 2D vdW magnets CrI<sub>3</sub> and CrBr<sub>3</sub> at low temperatures and robust down to monolayer. We realize field- and current-driven domain wall motion with velocities up to 1020 m s<sup>-1</sup>, which are comparable to the state-of-the-art materials for domain-wall based applications [Yang *et al.*, Nat. Nanotechnol. **10**, 221–226 (2015); Woo *et al.*, Nat. Mater. **15**, 501–506 (2016); Vélez *et al.*, Nat. Commun. **10**, 4750 (2019); Siddiqui *et al.*, Phys. Rev. Lett. **121**, 057701 (2018); Ryu *et al.*, Nat. Nanotechnol. **8**, 527–533 (2013)]. Domain walls keep their coherence driven by the spin-transfer torque induced by the current and magnetic fields up to large values of about 12 × 10<sup>9</sup> A cm<sup>-2</sup> and 5 T, respectively. For larger magnitudes of current or field, a transition to a hydrodynamic spin-liquid regime is observed with the emission of a periodic train of spin-wave solitons with modulational instability [Rabinovich and Trubetskov, *Oscillations and Waves: In Linear and Nonlinear Systems, Mathematics and its Applications* (Springer Netherlands, 2011)]. The emitted waveform achieves terahertz (THz) frequency in a wide range of fields and current densities, which opens up perspectives for reconfigurable magnonic devices. Moreover, we found that these spin-waves can transport spin angular momentum through the layers over distances as long as 10 μm without losses for the transport of spin information. Our results push the boundary of what is currently known about the dynamics of domain walls in 2D vdW ferromagnets and unveil strategies to design ultrathin, high-speed, and high-frequency spintronic devices.

Published under an exclusive license by AIP Publishing. <https://doi.org/10.1063/5.0062541>

## INTRODUCTION

Spin-based applications have been broadly explored for high-performance solid-state data storage technologies.<sup>18,19</sup> A promising strategy is to encode bits in magnetic domain walls, which can be controlled via applied magnetic fields and spin-polarized currents.<sup>4,9</sup> Several approaches for domain wall-based memory devices with a focus on the domain wall displacement have been developed. From a field-controlled shift register<sup>9,20</sup> up to the nonvolatile multi-turn sensors,<sup>21</sup> which are commercially available,<sup>22</sup> these emerging technologies provide a new horizon for advanced materials to be explored. With the discovery of magnetism in vdW layered compounds<sup>5–7</sup> and proof-of-concept devices<sup>8,23–25</sup> already showing outstanding progress toward applications, one of the main challenges is the integration of two-dimensional (2D) magnets in domain wall microelectronic platforms.<sup>1,3,10,11,15</sup>

Due to scaling reasons and high-density requirements,<sup>26</sup> competitive devices should have narrow domain walls (ideally in the range of 1–10 nm), use out-of-plane magnetic anisotropy materials, and in particular, for memory devices, develop domain wall velocities of the order of  $\sim 100$  m s<sup>-1</sup> to achieve rapid operating speed on increasing areal density.<sup>4,27</sup> Sufficiently low current densities ( $\sim 10^6$ – $10^8$  A cm<sup>-2</sup>) are also needed to guarantee low power consumption and to avoid damage due to Joule heating. However, metallic layers inherently suffer with energy dissipation via the conduction electrons,<sup>2</sup> which make magnetic insulators better suited for domain wall applications. There have been a few reports on the creation of different interfaces using magnetic vdW materials<sup>28,29</sup> and heavy metal overlayers (e.g., Pt, Ta), where spin-transfer torque (SST) arising from charge-to-spin current conversion can effectively switch the magnetization from one state to another. Nevertheless, it is unknown how domain walls behave intrinsically in 2D magnets as currents and fields are applied directly into the systems, and how efficient such layered structures would be in domain-wall based functional devices.

Here, we demonstrate domain-wall motion in monolayer CrI<sub>3</sub> and CrBr<sub>3</sub> by spin polarized currents and magnetic fields in a broad range of densities ( $10^7$ – $10^9$  A cm<sup>-2</sup>) and fields (0.001–2 T). Both dynamics occur over hybrid domain walls with Néel–Bloch characteristics with a domain wall width of about  $\sim 5.30$  nm. The spin-torque induced by electric currents and magnetic fields generates a rapid rotation of the magnetization at the domain wall, hence triggering its translational motion at high velocities. We record speeds of up 1020 and 100 m s<sup>-1</sup> with current and field, respectively, while keeping the coherence of the wall profile through a steady motion. As the domain wall velocity approaches the maximum spin-wave group velocity, the domain wall motion starts to exhibit nonlinear effects with the emission of magnons at terahertz (THz) frequencies following a modulational instability (MI) behavior. Even though no conduction electrons are present in the medium due to the insulating characteristics of CrI<sub>3</sub> and CrBr<sub>3</sub>, spin-information can be transported over distances as long as 10  $\mu$ m, which sets a new paradigm for spin-wave-based technologies at the ultrathin limit.

## RESULTS

Our starting point is the investigation of the magnetic domain structures in monolayer CrBr<sub>3</sub> and their dynamic evolution under different temperatures and magnetic fields. The domain wall structure of CrI<sub>3</sub> and its cooling dynamics have recently been reported using similar theoretical frameworks.<sup>30</sup> We use a large square flake of  $0.4 \times 0.4 \mu\text{m}^2$  to represent a system able to be measured using

imaging techniques, i.e., nitrogen-vacancy scanning magnetometry.<sup>31</sup> We describe the interactions using the following spin Hamiltonian:

$$\mathcal{H} = - \sum_{ij} J_{ij} (\mathbf{S}_i \cdot \mathbf{S}_j) - \sum_{ij} \lambda_{ij} S_i^z S_j^z - \sum_i D_i (\mathbf{S}_i \cdot \mathbf{e}_i)^2 - \sum_{ij} K_{ij} (\mathbf{S}_i \cdot \mathbf{S}_j)^2 - \sum_i \mu_i \mathbf{S}_i \cdot (\mathbf{B}_i + \mathbf{B}_i^{\text{dp}}), \quad (1)$$

where  $\mathbf{S}_i$  and  $\mathbf{S}_j$  are the localized magnetic moments on Cr atomic sites  $i$  and  $j$ , which are coupled by pair-wise exchange interactions.  $J_{ij}$  and  $\lambda_{ij}$  are the isotropic and anisotropic bilinear (BL) exchanges, respectively, and  $D_i$  is the single ion magnetic anisotropy.  $\mathbf{B}_i$  and  $\mathbf{B}_i^{\text{dp}}$  represent external and dipole magnetic field sources, respectively. Equation (1) was previously found to describe accurately the magnetic properties of several 2D magnets<sup>30,32</sup> including CrI<sub>3</sub> and CrBr<sub>3</sub>. Comparisons with other spin Hamiltonians, such as Kitaev, bilinear Heisenberg, Ising, and Dzyloshinskii–Moriya interactions, were undertaken in Refs. 30 and 32 as well as in their [supplementary material](#). We take into account up to third nearest neighbors for  $J_{ij}$  and  $\lambda_{ij}$  in the description of CrBr<sub>3</sub> in Eq. (1). All the parameters in Eq. (1) are extracted using highly accurate non-collinear *ab initio* simulations taking into account spin-orbit coupling and the Hubbard- $U$  corrected density functional theory as described in Refs. 30 and 32. We ensure that fine numerical convergence within  $10^{-6}$ – $10^{-8}$  eV is achieved in each computed parameter. We also compared the exchange parameters used in our work with those collected from the literature.<sup>33</sup> In the context of the materials studied in our study (monolayer CrI<sub>3</sub> and CrBr<sub>3</sub>), [supplementary material](#) Fig. S1 clearly shows that our exchange magnitudes<sup>32</sup> reproduce with high accuracy the critical temperatures measured. Moreover, Eq. (1) provides an accurate description of the magnon dispersion extracted from inelastic neutron scattering measurements on CrI<sub>3</sub><sup>34</sup> as shown in Ref. 32. These results provide a firm background for the modeling of the domain wall dynamics as described here.

The fourth term in Eq. (1) represents the biquadratic (BQ) exchange, which involves the hopping of two or more electrons between two adjacent sites.<sup>32</sup> Its strength is given by the constant  $K_{ij}$ , which is the simplest and most natural form of non-Heisenberg coupling. It has recently been found that several 2D vdW magnets develop substantial BQ exchange in their magnetic properties, which are critical to quantitatively describe important features such as Curie temperatures, thermal stability, magnon spectra, and non-trivial topological spin textures.<sup>30,32,35,36</sup> The magnitude of  $K_{ij}$  for CrBr<sub>3</sub> is 0.22 meV, which is smaller than the BL exchange for the first-nearest neighbors ( $J_1 = 1.66$  meV) but still too sizable to be disregarded.<sup>32</sup> In our implementation, the BQ exchange is quite general and can be applied to any pair-wise exchange interaction of the arbitrary range. Each system is evolved by solving the atomistic Landau–Lifshitz–Gilbert equation with a Gilbert damping  $\lambda_G = 0.1$  to ensure better computational efficiency and numerical stability of the time integration. The value of  $\lambda_G$  is substantially higher than that ( $2 \times 10^{-3}$ ) recently measured for a parent compound<sup>37</sup> (i.e., CrCl<sub>3</sub>), in which a similar magnitude would be expected for CrI<sub>3</sub> and CrBr<sub>3</sub>. The large  $\lambda_G$  also accounts for the possibility of free-electron doping to raise the conductivity of the system due to different processes (i.e., dopants,<sup>38</sup> electric bias<sup>39</sup>). Due to the inclusion of dipole–dipole interactions, we explicitly include non-local

damping effects in our simulations such as due to domain walls or different magnetic textures. Hence, our spin-dynamics simulations include an accurate description of the spin-interactions at the atomic level (2–20 Å) in a multiscale framework at the lab scale (a few micrometers).

Monolayer CrBr<sub>3</sub> is thermally equilibrated above 40 K and then linearly cooled to 0 K in a total simulated time of 4.0 ns at different magnetic fields (Fig. 1 and [supplementary material](#) movies S1–S4). The time evolution of the out-of-plane magnetization  $M_z$  is utilized to study the nucleation of the magnetic domains as it determines the easy-axis throughout the layer. For zero-field cooling (0 mT), magnetic domains are formed for temperatures below 20 K with the free motion of the domain walls as the temperature drops [Figs. 1(a)–1(e)]. As the system reaches 0 K, a continuous time evolution of the domain

structures remains, which results in a homogenous magnetization over the entire crystal ([supplementary material](#) movie S1). Even though thermal fluctuations as well as their contributions to the energy of the system are inexistent at 0 K, other terms, such as dipolar fields, exchange interactions, and magnetic anisotropy, are still present, further contributing to the modification of the magnetic domains. Once magnetic fields are applied to the nanosheet [Figs. 1(f)–1(t) and [supplementary material](#) movies S2–S4], this nucleation-type mechanism is accelerated with a rapid reversal in the sign of the magnetization  $M_z$ . Indeed, a monodomain feature is observed even in fields far below the coercivity<sup>40</sup> (10 mT at 5 K) for CrBr<sub>3</sub>. In a scenario where defects or pinning sites are not present in monolayer CrBr<sub>3</sub>, magnetic domains tend to be metastable with a homogeneous magnetization throughout the surface. This is in sound agreement with recent NV-center

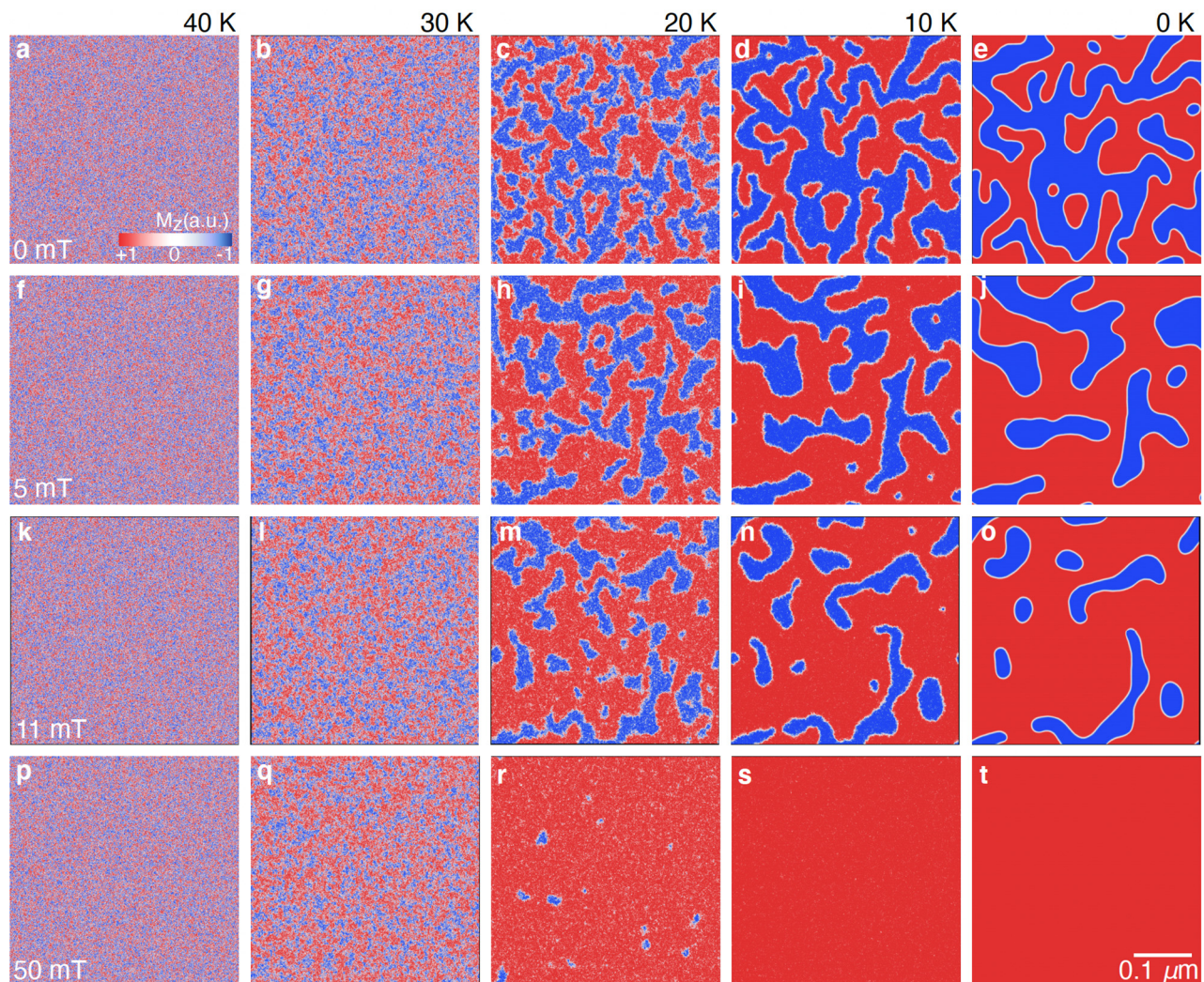


**FIG. 1.** Magnetic domains at different temperatures and fields. (a)–(e) Dynamical spin configurations of monolayer CrBr<sub>3</sub> during zero-field cooling (0 mT) at different temperatures. The out-of-plane magnetization  $M_z$  (a.u.) is used to follow the evolution of the magnetic domains from 40 K down to 0 K. [(f)–(j), (k)–(o), and (p)–(t)] Similar as (a)–(e), but at magnetic fields of 5, 11, and 50 mT, respectively. Temperatures at the top row correspond to all panels in the same column. Time scale spanned up to 2.5 ns till 0 K is achieved. Further evolution is observed at later times as shown in [supplementary material](#) movies S1–S4.

scanning magnetometry measurements<sup>31</sup> on the magnetic domain evolution of CrBr<sub>3</sub>, indicating that pinning effects are the dominant coercivity mechanisms.

Strikingly, the interplay between domain metastability and high magnetic anisotropy of CrBr<sub>3</sub> gives additional characteristics to the domain walls [Figs. 2(a)–2(b)]. We observe that as the spins vary orientation from one magnetic domain to another, the wall profile assumes components of the magnetization along different in-plane directions ( $M_{x,y}$ ) relative to the easy-axis ( $M_z$ ) [Figs. 2(c)–2(d)]. In-plane magnetization  $M_x$  displays a variation larger than that for  $M_y$ , which is mainly noticed at the core of the domain wall within 1–2.5 nm. These features indicate a domain wall with hybrid characteristics of Bloch and Néel type [Figs. 2(e)–2(f)]. We can extract the domain wall width  $\sigma_{x,y,z}$  by fitting the different components of the magnetization ( $M_x$ ,  $M_y$ ,  $M_z$ ) to standard equations of the form<sup>41</sup>

$$M_j = \frac{1}{\cosh(\pi(j - j_0)/\sigma_j)}, \quad \text{with } j = x, y, \quad (2)$$

$$M_z = \tanh(\pi(z - z_0)/\sigma_z), \quad (3)$$

where  $j_0$  and  $z_0$  are the domain wall positions at in-plane and out-of-plane coordinates, respectively. The domain wall widths are within the range of  $\sigma_{x,y,z} = 5.30 - 5.33$  nm. Materials with high magnetic anisotropy generally stabilize such small domain wall widths, but their magnetic domains are generally stable after zero-field cooling due to long range dipole interactions. We have checked that the inclusion of dipolar fields in our simulations do not change the results.

An intriguing question raised by the hybrid features of the domain walls in CrBr<sub>3</sub> and CrI<sub>3</sub><sup>30</sup> is the effect of magnetic fields and electric currents on the motion of domain walls. It is well established that both driving forces can induce displacement of domain walls in magnetic thin films over different substrates. Nevertheless, the vdW

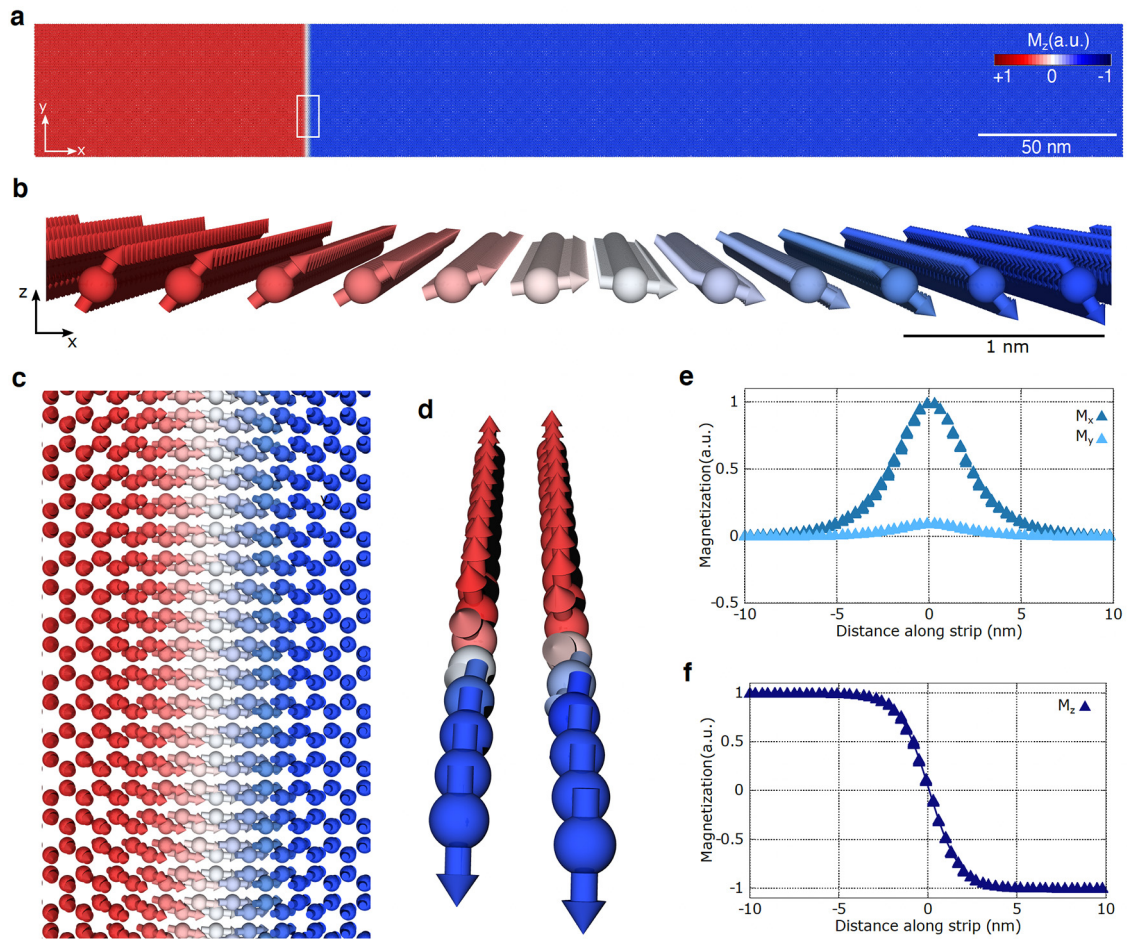


**FIG. 2.** Hybrid domain walls with Néel–Bloch characteristics. [(a) and (b)] Global and local views, respectively, of a snapshot for one of the spin configurations projected along  $M_z$  (color map) showing the formation of a domain wall in monolayer CrBr<sub>3</sub>. The total strip in (a) is  $400 \times 50$  nm. Only Cr atoms are shown in the honeycomb lattice arrangement of monolayer CrBr<sub>3</sub>. The system is at 0 K without any external fields or currents. [(c) and (d)] Side and top views, respectively, of the rotation of the magnetization along the domain wall. Both  $M_x$  and  $M_y$  show variations along the wall altogether with  $M_z$ , which indicate a hybrid character of the domain wall with Néel and Bloch features. Colors follow the scale bar in (a). The small area around the domain wall highlighted in (a) corresponds to (c). [(e) and (f)] Variation of the magnetization along the domain wall projected along the in-plane components ( $M_x$ ,  $M_y$ ) and  $M_z$ , respectively. Fitting lines are obtained using Eqs. (2) and (3).

nature of the nanosheet together with the atomic thickness ( $\approx 0.5$  nm) may induce additional phenomena yet to be observed in 2D ferromagnets. Figures 3(a)–3(d) show that either fields or currents can efficiently displace domain walls in layered CrBr<sub>3</sub> and CrI<sub>3</sub> magnets. The dynamics is generally initialized with a domain wall at the equilibrium position previously thermalized for several nanoseconds for full convergence of the spin orientations [Fig. 3(a)]. The finite width of the nanowire assists in the formation of the domain walls pinned by the edges. For field-induced domain wall motion, wall velocities up to  $v = 70$  and  $v = 98$  m s<sup>-1</sup> are recorded for CrBr<sub>3</sub> and CrI<sub>3</sub> [Figs. 4(a) and 4(b)], respectively. The wall moves steadily on both sheets and can be described as  $v = \mu_F(B - B_0)$ , where  $\mu_F$  is the wall mobility and  $B_0$  is the onset field required to move the wall from structural defects or pinning.<sup>42</sup> The magnitudes of  $\mu = 0.0343$  m s<sup>-1</sup>mT<sup>-1</sup> and  $B_0 = 23.89$  mT for CrBr<sub>3</sub> and  $\mu = 0.018$  m s<sup>-1</sup>mT<sup>-1</sup> and  $B_0 = 13.33$  mT for CrI<sub>3</sub> indicate that domain walls move relatively slower than those in metallic ultrathin Pt/Co/Pt films<sup>43</sup> or thick magnetic insulator

TmIG/Pt interfaces<sup>14</sup> but with relatively similar onset field  $B_0$ . The domain wall moves steadily on both sheets at fields below critical magnitudes ( $B_c$ ) of  $B_c = 1.19$  T and  $B_c = 4.78$  T for CrBr<sub>3</sub> and CrI<sub>3</sub>, respectively (supplementary material movies S5 and S6). For values beyond  $B_c$ , different spin distributions start nucleating ahead of the domain-wall (supplementary material movies S7 and S8) and induce its collapse within a few hundreds of picoseconds after the motion initiated. These spin features appear from the edges of the layers and rapidly move into the bulk of the ribbon. This behavior is analogous to that observed in Pt/Co/AlO<sub>x</sub> ultrathin microstructures<sup>44</sup> and highlighted the importance of edges on the magnetic properties of 2D magnets in device integration. A preference for unreconstructed edges or dangling bonds rather than on zigzag edges [Fig. 3(b) at 1.50 T] has been observed in the nucleation of reversed domains during the wall dynamics. The local variation of the exchange interactions at dangling-bonds with spins being less restricted to change their directions with an external field than at zigzag edges is one of

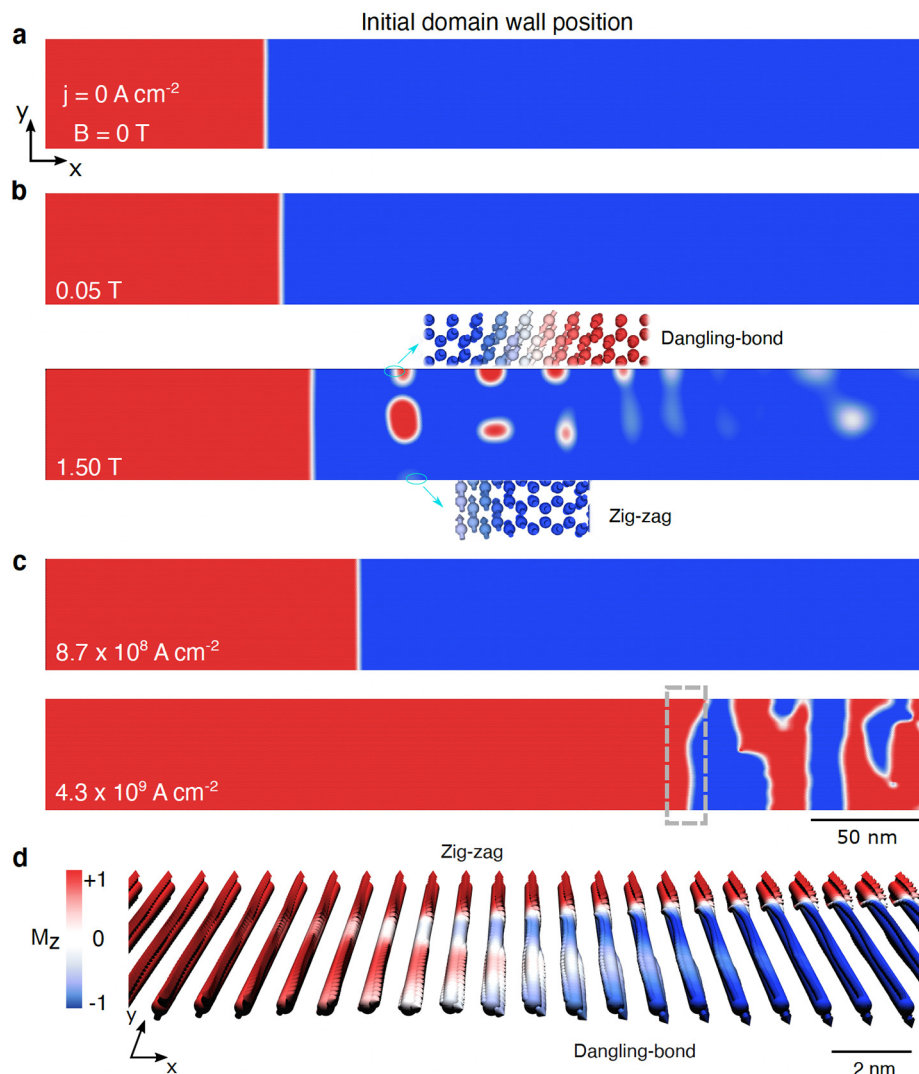


**FIG. 3.** Current- and field-induced domain wall dynamics in 2D ferromagnets. (a) Initial domain wall configuration for monolayer CrBr<sub>3</sub> at no external driving forces ( $j = 0$ ,  $B = 0$ ). The domain wall is initially equilibrated for up to 4 ns to ensure convergence of the spin orientations along the wall and width. The same final configuration is utilized for both field- and current-driven domain wall motion. Similar procedure is undertaken to monolayer CrI<sub>3</sub>. [(b) and (c)] Snapshots of the domain wall dynamics in CrBr<sub>3</sub> induced by magnetic fields (0.05, 1.50 T) and electric currents ( $8.7 \times 10^9$  A cm<sup>-2</sup>,  $4.3 \times 10^9$  A cm<sup>-2</sup>), respectively. The edges used in the simulations are highlighted at  $B = 1.50$  T with dangling-bond and zigzag at the top and bottom of the layer, respectively. Deformations observed near the domain wall at  $j = 4.3 \times 10^9$  A cm<sup>-2</sup> are highlighted by the dashed rectangle. (d) Zoom-in of the local spin-configurations at  $j = 4.3 \times 10^9$  A cm<sup>-2</sup> with color scale showing the variations of the spin orientations along  $M_z$  induced by the large current density.

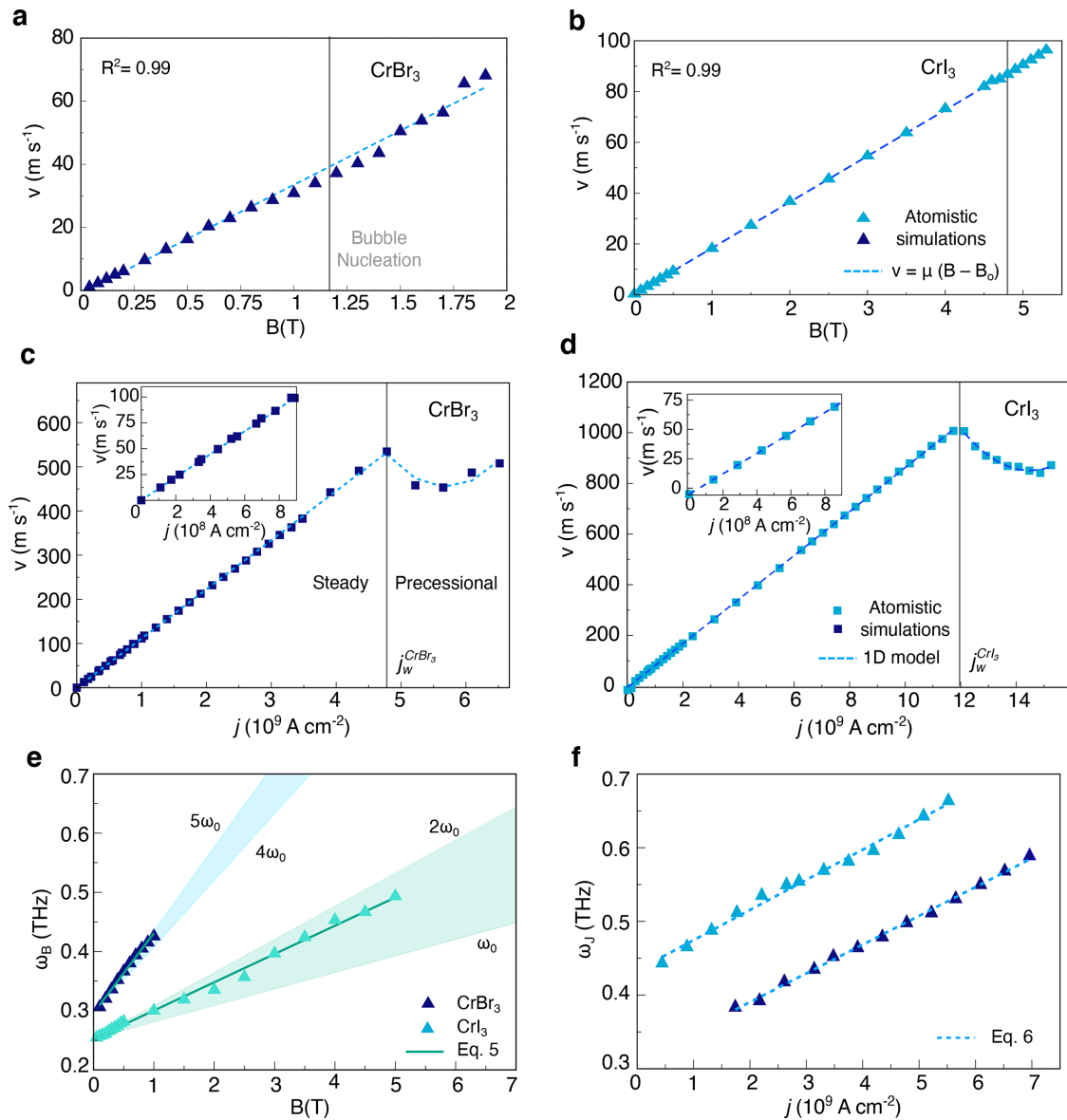


**FIG. 4.** Domain wall speeds and spin wave frequency. [(a) and (b)] Calculated domain wall velocities  $v$  vs the applied magnetic field  $B$  for CrBr<sub>3</sub> and CrI<sub>3</sub>, respectively. The vertical solid lines indicate the region where the nucleation of magnetic bubbles starts in each material as those shown in (b) at 1.50 T for CrBr<sub>3</sub>. A fit using  $v = \mu(B - B_0)$ , where  $\mu$  is the domain wall mobility and  $B_0$  is the onset field, reproduces accurately the atomistic simulation data with linear regression coefficients  $R^2 = 0.99$  and a root-mean-square-error of 0.0074. The field is applied perpendicular to the surface following the easy-axis of the materials. [(c) and (d)] Variations of  $v$  as a function of the current density  $j$  for CrBr<sub>3</sub> and CrI<sub>3</sub>, respectively. Two regimes are observed in the internal dynamics of the wall before and after the Walker breakdown ( $j_w$ ) with the wall motion being in steady and precessional states, respectively. We could extract  $j_w^{CrBr_3} = 4.8 \times 10^9$  A cm<sup>-2</sup> and  $j_w^{CrI_3} = 12.0 \times 10^9$  A cm<sup>-2</sup>. Both steady and precessional regimes on the domain-wall dynamics can be modeled using a 1D model as described in the text. The insets show the velocities at lower values of current within  $j < 8.5 \times 10^8$  A cm<sup>-2</sup>. [(e) and (f)] Frequencies  $\omega_B$  (THz) and  $\omega_J$  (THz) of the emitted spin-waves during the domain-wall motion as a function of  $B$  and  $j$ , respectively, for CrBr<sub>3</sub> and CrI<sub>3</sub>. Dashed lines are corresponding fits to Eqs. (5) and (6). Similar data labeling applies for (e) and (f).

the main ingredients for this behavior. This observation shall trigger further experimental studies of the atomic structure at the edges of the monolayer magnets via scanning probe microscopies<sup>45,46</sup> and their connection to the device performance.

In the case of current-driven domain wall motion, we state that such a behavior can be accomplished in two ways: first, by using an

adjacent conducting layer as recently demonstrated for insulating Tm<sub>3</sub>Fe<sub>5</sub>O<sub>12</sub> on top of a Pt substrate.<sup>14</sup> Charge current will flow in the heavy metal generating spin currents that exert a spin-transfer torque (STT) on the ferromagnetic material. Second, by doping the CrX<sub>3</sub> (X = Br, I) magnets in order to generate significant carriers in the host.<sup>27,47</sup> Such strategies are well established and would provide a

feasible platform to confirm our predictions. Indeed, we recorded domain wall velocities up to  $530 \text{ m s}^{-1}$  and  $1020 \text{ m s}^{-1}$  for monolayers  $\text{CrBr}_3$  and  $\text{CrI}_3$ , respectively, under applied currents [Figs. 4(c) and 4(d)]. These velocities are higher than those observed in a wide range of systems including skyrmions ( $100 \text{ m s}^{-1}$ ),<sup>13</sup> ferromagnetic semiconductors (Ga, Mn)As ( $22 \text{ m s}^{-1}$ ),<sup>47</sup> synthetic antiferromagnets ( $750 \text{ m s}^{-1}$ ),<sup>12</sup> metallic layers ( $380 \text{ m s}^{-1}$ ),<sup>48</sup> Pt/CoFe/MgO and Co/Ni/Co interfaces ( $\sim 10 \text{ m s}^{-1}$ ,  $400 \text{ m s}^{-1}$ ),<sup>16,49</sup> and insulating oxides ( $400 \text{ m s}^{-1}$ ).<sup>14</sup> It is worthwhile to highlight that low current densities within the experimental range of  $10^{-8} \text{ A cm}^{-2}$  [insets in Figs. 4(c) and 4(d)] already resulted in domain wall speeds (i.e.,  $100 \text{ m s}^{-1}$ ) similarly as those achieved in established racetrack platforms with more complex materials.<sup>4</sup> The domain walls displace freely as a function of the current density  $j$  in a viscous flow motion (supplementary material movies S9 and S10). The high velocities predicted for  $\text{CrBr}_3$  and  $\text{CrI}_3$  are only limited by the spin-wave group velocity  $v_g$  intrinsic to the systems. By using a spin-wave theory for 2D magnetic materials,<sup>32</sup> which includes biquadratic exchange and Dzyaloshinskii–Moriya interactions (DMI), we estimate from the magnon dispersion (supplementary material, Fig. S2) the maximum values of  $v_g$  within the range of  $584\text{--}891 \text{ m s}^{-1}$  for  $\text{CrBr}_3$  and  $1326\text{--}6400 \text{ m s}^{-1}$  for  $\text{CrI}_3$  (supplementary material Fig. S3). These values are close to those computed from the atomistic simulations ( $530$  and  $1020 \text{ m s}^{-1}$  for  $\text{CrBr}_3$  and  $\text{CrI}_3$ , respectively) although slightly larger. This is due to the damping of the domain wall motion by the emission of spin-waves<sup>50</sup> not taken into account into the model as commented in the following.

The steady displacement of the domain walls occurs up to a certain threshold ( $j_w$ ) defined as the Walker breakdown.<sup>42</sup> For values below  $j_w$  the wall dynamics can be well modeled by a simple 1D model<sup>51,52</sup> through a linear dependence of  $v$  and  $j$ ,

$$v = \mu_I j, \quad (4)$$

where  $\mu_I$  is the current-driven domain-wall mobility, which gives  $\mu_I = 0.12 \times 10^{-10} \text{ m}^3 \text{ A}^{-1} \text{ s}^{-1}$  and  $\mu_I = 0.10 \times 10^{-10} \text{ m}^3 \text{ A}^{-1} \text{ s}^{-1}$  for monolayers  $\text{CrBr}_3$  and  $\text{CrI}_3$ , respectively. These values are of the same order of magnitude as those recorded on thin metallic interfaces<sup>49</sup> or Permalloy nanowires,<sup>53</sup> which have been studied more intensively. For values near  $j_w$  or above, the spins at the domain wall precesses inducing disruption of the wall at longer times with the nucleation of magnetic domains with a different polarization ahead of the displacement of the domain-wall [Fig. 3(c) at  $4.35 \times 10^9 \text{ A cm}^{-2}$ ]. A close look at these features [Fig. 3(d)] indicates that they may start from both edges although dangling-bonds may induce more curvature to the domain wall since a dragging on the motion is observed generating retardation relative to the zigzag edge. We can model qualitatively the dynamics at  $j > j_w$  for both  $\text{CrBr}_3$  and  $\text{CrI}_3$  via the time average velocity of the domain wall.<sup>51,52</sup> This suggests that the domain-wall dynamics in 2D magnets is similar to that in magnetic nanowires, which allows faster integration into existing devices.<sup>27</sup> We also observe that as the domain wall moves, spin-waves or magnons are emitted [Figs. 4(e)–4(f)]. The spin frequencies driven by the field ( $\omega_B$ ) and current ( $\omega_J$ ) are in the terahertz (THz) regime with maximum magnitudes of  $\omega_B^{\text{max}} = 0.43 \text{ THz}$  and  $\omega_J^{\text{max}} = 0.60 \text{ THz}$  for  $\text{CrBr}_3$  and  $\omega_B^{\text{max}} = 0.50 \text{ THz}$  and  $\omega_J^{\text{max}} = 0.66 \text{ THz}$  for  $\text{CrI}_3$ . These frequencies are in sound agreement with those estimates from the magnon dispersion along different points of the Brillouin zone for both halides (supplementary material Fig. S3). We found that the maximum frequencies with the field are

close to those at the M-point ( $0.47 \text{ THz}$  for  $\text{CrBr}_3$  and  $0.57 \text{ THz}$  for  $\text{CrI}_3$ ), whereas with the applied current are around the K-point ( $0.63 \text{ THz}$  for  $\text{CrBr}_3$  and  $0.64 \text{ THz}$  for  $\text{CrI}_3$ ). Indeed, the variations of  $\omega_B$  and  $\omega_J$  can be well fitted using

$$\omega_B = \omega_0^B + \alpha_B B, \quad (5)$$

$$\omega_J = \omega_0^J + \alpha_J j, \quad (6)$$

where  $\omega_0^B (B = 0)$  and  $\omega_0^J (j = 0)$  are the onset frequencies resulting in  $\omega_0^B = 0.29 \text{ THz}$  and  $\omega_0^J = 0.31 \text{ THz}$  for  $\text{CrBr}_3$ ; and  $\omega_0^B = 0.25 \text{ THz}$  and  $\omega_0^J = 0.43 \text{ THz}$  for  $\text{CrI}_3$ . We also notice that the magnitudes of  $\omega_0^B$  and  $\omega_0^J$  may also change due to the inhomogeneous spatial distribution of the emitted spin-waves (supplementary material movie 11) even though with a similar behavior with the field and current. The coefficient  $\alpha_B$  differs moderately between both halides converging to  $0.13$  and  $0.05 \text{ THz T}^{-1}$  for  $\text{CrBr}_3$  and  $\text{CrI}_3$ , respectively, with  $\alpha_J \approx 0.04 \text{ THz } 10^{-9} \text{ A cm}^{-2}$  being similar to both systems. On the field-driven spin-wave emission, the domain wall precesses with a frequency near the Larmor frequency  $\omega_0 = \gamma B$ , where  $\gamma$  is the gyromagnetic ratio, similarly as in nanowires.<sup>54</sup> We noticed that in both layered materials, the spin wave frequencies are enclosed between odd- and even-numbered harmonics. That is,  $\text{CrBr}_3$  is within  $4\omega_0$  and  $5\omega_0$  ( $\omega_B - \omega_0^B = 4.81\omega_0$ ), and  $\text{CrI}_3$  is within  $\omega_0$  and  $2\omega_0$  ( $\omega_B - \omega_0^B = 1.70\omega_0$ ). This indicates that the spin waves and their overtones can be excited with a combination of fundamental modes, which gives additional flexibility for terahertz source of the magnetic signal using atomically thin layers. In addition, the emission of spin waves electrically driven can be associated with the Doppler effect on the frequency shift.<sup>55</sup> As the domain wall moves, the current changes the spin-waves dispersion and incidentally causes an effective flow of the magnetic medium. This is reflected by the linear dependence of  $\omega_J$  on  $j$  [Fig. 4(f)] in agreement with the spin-transfer-torque Doppler shift. A similar approach has been successfully used to study the effect of an electric signal into magnons in Permalloy strips,<sup>56</sup>  $\text{Ni}_{80}\text{Fe}_{20}$  wires,<sup>57</sup> and thin films.<sup>58</sup>

A substantially different phenomenon is observed when the domain wall is subject to large current densities,  $j > 10^{10} \text{ A cm}^{-2}$ , with the appearance of spin hydrodynamic effects in  $\text{CrBr}_3$  and  $\text{CrI}_3$ . The dynamics is illustrated in Figs. 5(a)–5(c), where we plot line-cuts of the  $M_z$  and  $M_x$  components of the magnetization at width  $25 \text{ nm}$ , and selected times for monolayer  $\text{CrI}_3$ . We observe that shortly after the electric pulse starts propagating into the system within  $18\text{--}78 \text{ ps}$ , the  $M_x$  projection exhibits a wave propagating ahead of the domain wall. This amplitude tilts  $M_z$  into the plane and increases exponentially [Fig. 5(d)] until  $M_z$  is completely suppressed and eventually switches, nucleating a new domain wall. The first period of the wave in  $M_x$  or a shock wave (SW) continues to propagate with no appreciable dissipation, and new domain walls are nucleated in its wake with a certain periodicity [Figs. 5(a)–5(c)]. This nonlinear phenomenon is indicative of a modulational instability (MI) as observed in fluid dynamics.<sup>17,59</sup> This type of instability occurs in focusing media and describes the exponential growth of waves within a band of wavevectors until nonlinear effects favor their spatial localization into solitons. MIs are ubiquitous in dispersive physical problems and have been observed in several systems such as in water waves,<sup>60</sup> nonlinear optics,<sup>61</sup> and Bose–Einstein condensates.<sup>62</sup> In magnetic materials, however, MI has been invoked so far as a pathway for the nucleation of dissipative



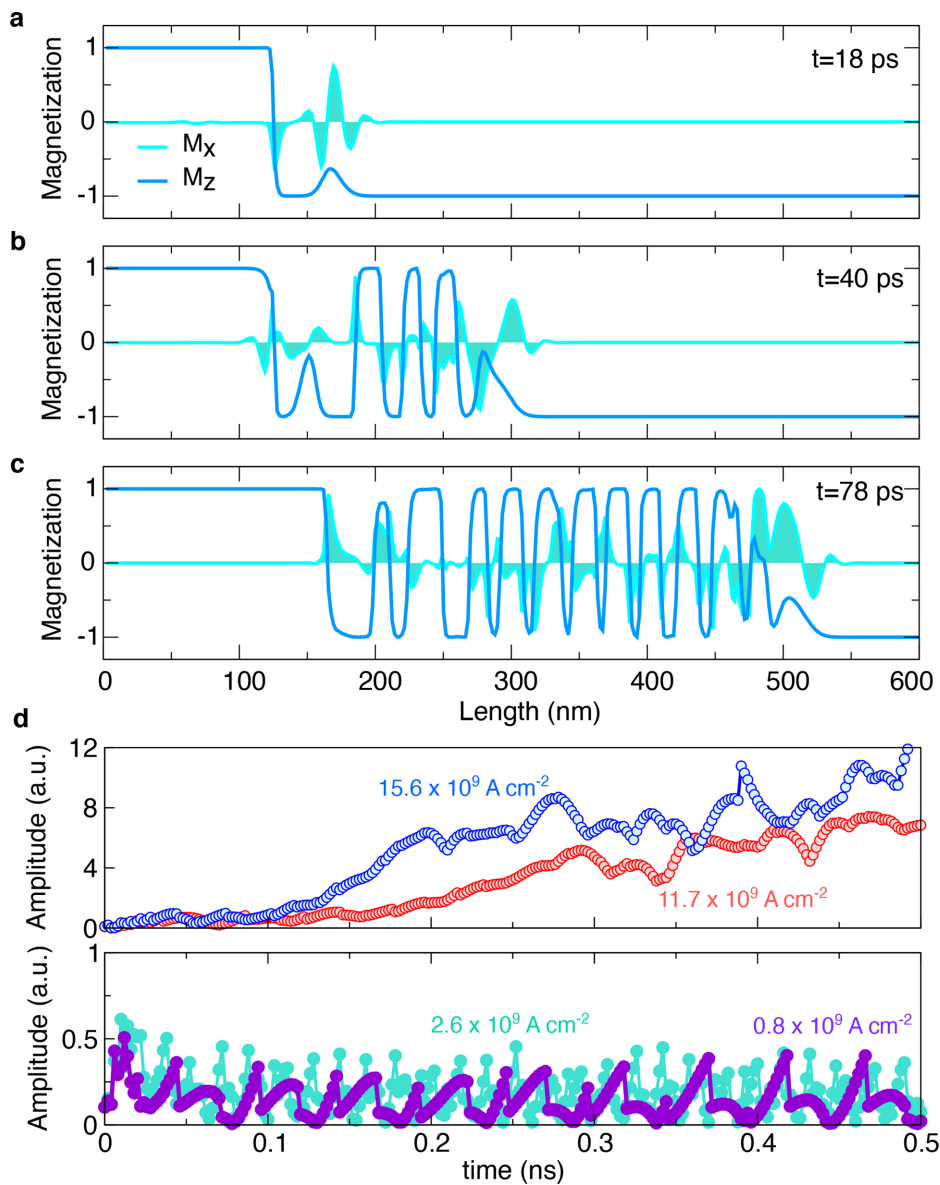


**FIG. 5.** Modulation instability in 2D magnets. [(a)–(c)] Snapshots of the magnetization along  $M_z$  and  $M_x$  magnetization components at different times at 18, 40, and 78 ps, respectively. (d) Amplitude of  $M_x$  as a function of time at different current densities.

droplets in perpendicular magnetic anisotropy (PMA) ferromagnets,<sup>63</sup> as well as the spatial localization of high-energy magnons in PMA ferromagnetic alloys excited with ultrafast optical pulses,<sup>64</sup> and the disintegration of short-wavelength spin-superfluids in planar ferromagnets.<sup>65</sup> In contrast, we find clear evidence of spin hydrodynamic behavior manifested the onset of MI and its nonlinear dynamics driven by electrical currents in 2D magnetic materials. We emphasize that the nonlinear effect observed here is fundamentally different from Walker breakdown and the subsequent precessional regime so far observed in bulk magnets.

We also observe that MI is visible already at 20 ps as the wavefront exhibits a transverse structure and can be more generally regarded as a spin shock wave [Figs. 6(a)–6(c)]. At 200 ps, there are

rich transverse features in the nanoribbon, from which we can identify a modulationally unstable region where new domains are established. These domains are bounded by the trailing domain-wall (soliton edge) and the spin shock wave. At 600 ps, the shock wave is already outside our simulation profile, and the domain walls continue to propagate further (see the [supplementary material](#) movie S12 for the full sequence). The salient features of the MI dynamics can be visualized in Fig. 6(d) by a color-plot of the  $M_z$  component line-cuts as a function of time. After an initial translation of the domain wall, there is a split of behaviors at  $\approx 0.01$  ns, where we can define two characteristic speeds [dashed lines in Fig. 6(d)]. The shock wave (SW) [Fig. 6(b)] translates with a speed of  $s^+ = 5.77 \pm 0.84 \text{ km s}^{-1}$ , which is in sound agreement with the maximum group velocity calculated for CrI<sub>3</sub>

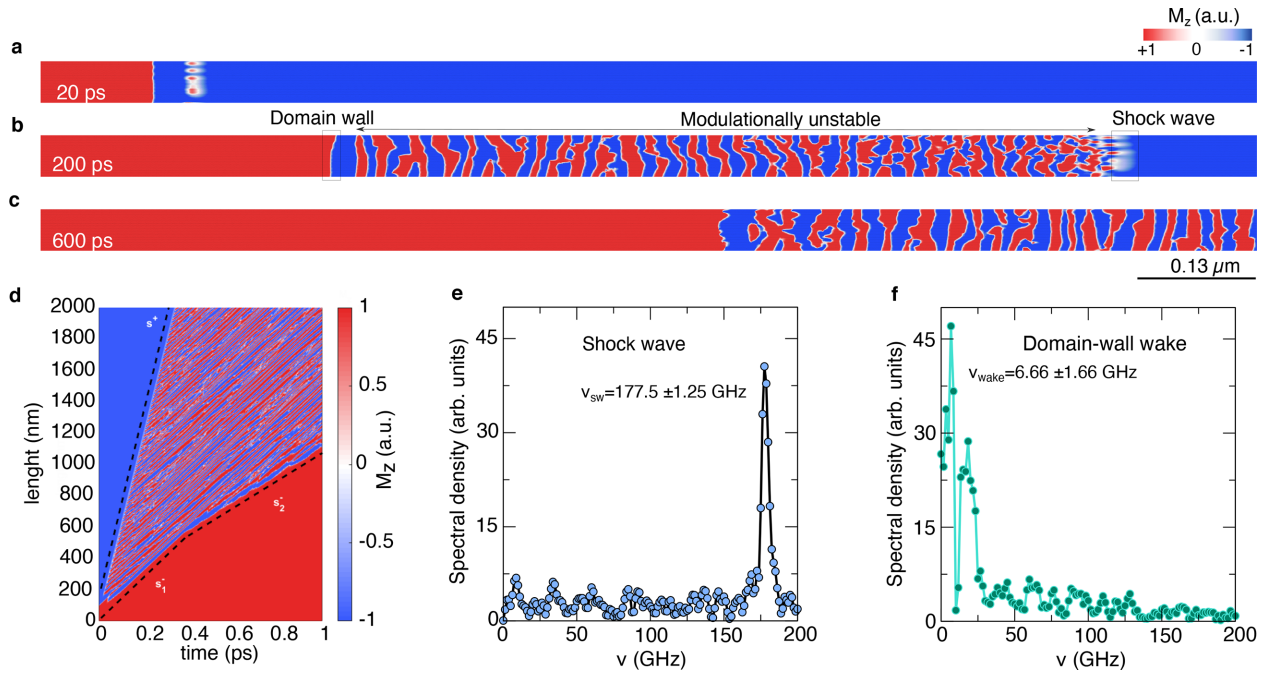


**FIG. 6.** Long range spin-wave propagation. [(a)–(c)] Snapshots of spin-dynamics at 20, 200, and 600 ps, respectively, under a current density of  $1.56 \times 10^{10}$  A cm $^{-2}$ .  $M_z$  is used to show the variations of the domain wall with the color scale along the length of the ribbon. A separation of the motion of the original domain wall (soliton edge) and the shock waves can be observed between a wave train (modulationally unstable) propagating throughout the system. (d) Color-plot of the variations of  $M_z$  with the propagation time along a 2- $\mu$ m ribbon of CrBr $_3$  at a current density of  $1.56 \times 10^{10}$  A cm $^{-2}$ . The different line-cuts correspond to the several waveforms moving into the systems as shown in (e)–(g). The dashed lines are given by  $s^+ = 5773 \pm 0.84$  m s $^{-1}$ ,  $s_1^- = 1328 \pm 1.7$  m s $^{-1}$ , and  $s_2^- = 882 \pm 1.8$  m s $^{-1}$ . [(e) and (f)] Spectral density (arb. units) extracted from the fast Fourier transform of the  $M_z$  component as a function of time in (d) along velocities  $s^+$  and  $s_2^-$ , respectively. The characteristic frequencies of the shock waves and the domain-wall wake can be identified as  $\nu_{SW} = 177.5 \pm 1.25$  GHz and  $\nu_{wake} = 6.66 \pm 1.66$  GHz, respectively.

(supplementary material Fig. S3). The soliton edge exhibits a phase-shift and subsequent translation with a speed of  $s_1^- = 1.33 \pm 0.002$  km s $^{-1}$  [Fig. 6(b)]. Consequently, the wavelength  $L$  of the nucleated domains can be extracted from the spectral function at a constant speed such as  $s^+$  [Fig. 6(e)]. The obtained frequency of the wavefront or SW is computed as  $\nu_{SW} = 177.5 \pm 1.25$  GHz. We can immediately extract  $L$  through a simple speed and frequency relationship via  $L = s^+ / \nu_{SW} = 5.77$  km s $^{-1} / 177.5$  GHz =  $32.50 \pm 0.23$  nm, which is equivalent to a wave-vector of  $k_{SW} = 2\pi/L = 0.19 \pm 0.00003$  nm $^{-1}$ . Indeed, the shock-wave speed corresponds to the group velocity of the most unstable magnon with a wave-vector given by  $k_{SW}$ .

The growing region bounded by the speeds  $s^+$  and  $s_1^-$  is reminiscent to the development of dispersive shock waves (DSWs),<sup>17</sup> which are located at the modulationally unstable region highlighted in Fig. 6(b). DSWs are ordered structures that smoothly connect the wavevectors at the front and soliton edges and have been fully characterized for planar ferromagnets.<sup>66</sup> However, the MI in our system induces periodic domain-wall nucleation defined by the most unstable wavevector. Therefore, we can regard the scenario of Figs. 6(b) and 6(c) as an unstable generalization of a DSW. The periodicity of the nucleated domains leads to initially similar domain-wall speeds (parallel features in the wake of the wavefront) that are later perturbed by interactions, annihilation, and nucleation events. These can be potentially related to turbulence, thermodynamic behavior as a soliton gas,<sup>67</sup> or rare events such as rogue waves.<sup>60</sup> At a later time ( $\approx 0.04$  ns), a

second characteristic domain-wall speed  $s_2^- = 0.88 \pm 0.001$  km s $^{-1}$  is observed. This second speed appears to be related to an additional source of MI in the wake of the soliton-edge that opposes the current-driven torque. We can extract the frequency of this domain-wall wake [Fig. 6(f)] resulting in  $\nu_{wake} = 6.66 \pm 1.66$  GHz. Given the value of  $s_2^-$ , we can extract a wavelength of  $132.28 \pm 32$  nm, which corresponds to the periodicity of where new domain wall appears into the system induced by the wake of the domain-wall motion.

Interestingly, we also found that, in principle, there is no spatial limit for the propagation of the shock waves in the systems. Simulations undertaken at a mesoscopic level (supplementary material Fig. S4) showed that once an electrical excitations is applied into the system, the transmission of short-wavelength spin waves can extend for long-distances with minor disturbance from the medium. We record lengths up to 10  $\mu$ m with a group velocity above  $\sim 2000$  m s $^{-1}$ , where spin-waves can work as nanoscale information carriers. The spatial distance is at the same order of magnitude as those previously obtained in the magnetic insulator yttrium iron garnet (YIG)<sup>68</sup> and ferromagnetic nanowires grown on a thick YIG thin-film<sup>69</sup> with both have been proposed as platforms to controllable transmission of spin information. The combination between small damping ( $\approx 2 \times 10^{-3}$ ) in this class of 2D ferromagnets,<sup>37</sup> the insulating nature of CrI $_3$  and CrBr $_3$  with no conduction electrons available to induce decay in the spin signal,<sup>70</sup> and the relative low magnon scattering<sup>71</sup> make magnetic layered materials a new endeavor for magnonics applications.

## DISCUSSION

The possibility to manipulate and control domain walls precisely on 2D vdW CrX<sub>3</sub> (X = Br, I) magnets opens up a pathway to design a range of novel and highly competitive applications in the thickness of a few atoms. As some of the critical parameters to domain-wall based devices are domain wall widths, which control the information density, domain wall motion, directly governing access time, and pinning processes, that determine the energy consumption, 2D magnets show features that are fundamental for integration in novel memory technologies such as racetrack memories.<sup>4</sup> The large domain wall speeds achieved in both CrBr<sub>3</sub> and CrI<sub>3</sub> at the limit of 1020 m s<sup>-1</sup> compete side-by-side with the best materials used for racetrack applications (e.g., synthetic antiferromagnets<sup>12</sup>), where complex interfaces need to be fabricated to induce fast domain wall shifting. This remarkable result, along with recent advances in the scalable bottom-up growth of CrX<sub>3</sub> in the monolayer regime,<sup>72,73</sup> clearly presents as an opportunity for reduction in manufacturing and time-consuming device preparation. There is still a challenge that needs to be overcome to enable current-driven excitations in these 2D magnetic halides, for instance, the enhancement of the conductivity and the consequent reduction in the current densities used to move domain walls. One route is to use doping, which is a well-known strategy that has been widely employed in other prototypical ferromagnetic semiconductors [such as (Ga,Mn)As].<sup>47</sup> In fact, carrier doping has been found to induce half-metallicity and enhance the ferromagnetic stability in the CrI<sub>3</sub> monolayer,<sup>39,74</sup> such that current-induced phenomena become feasible without compromising the magnetic properties. It is worth mentioning that some trade-offs between conductivity enhancement and dissipation through the conduction electrons would have to be achieved for low-power consumption. It is well known that large Gilbert damping  $\lambda_G$  allows fast relaxation of the magnetization to equilibrium, whereas low damping enables energy-efficient processes. Several approaches<sup>75–78</sup> were previously developed on metallic systems that may assist in the pursue of the modeling of conduction electrons on doped-2D magnets. If the electrical conductivity of CrX<sub>3</sub> (X = I, Br) is enhanced due to different chemical or physical processes, the values of the domain wall speeds shown in Fig. 3 would be robust against such variations. Since the magnitude of the Gilbert damping  $\lambda_G$  utilized in the simulations ( $\lambda_G = 0.10$ ) is higher than that expected for CrI<sub>3</sub> and CrBr<sub>3</sub>,<sup>37</sup> we intrinsically take into account additional dissipation effects in our simulations. Furthermore, investigations to clarify the effect of different dopants, concentrations, and their implications on both damping and the magnetic properties of 2D magnets are promptly needed. The emission of spin waves in the THz regime and the spin hydrodynamic behavior observed for both halides, also merit further exploration on novel information technologies. On the one hand, the design of sources, detectors, and prototypes functioning in the THz-gap (0.3–30 THz)<sup>79</sup> provides the groundwork for the developments of high-end electronics on the low-end of the electromagnetic spectrum. The ultrathin character of 2D magnets, their flexibility in generating tunable frequencies, and inexpensive sample cost relative to expensive bulky compounds<sup>79</sup> make vdW layered materials a playground for applications. On the other hand, the use of magnons for information carriers at the  $\mu\text{m}$ -scale puts vdW sheets in the roadmap of post-semiconductor spin-wave technologies. The characteristic soliton features observed on the shock-waves in both ferromagnets and consequent low dissipation indicate that magnon-based data operations

may be explored for information processing. In this sense, the development of an energy-efficient spin-wave transducer through vdW materials is one of the key steps for the ultimate goal of hybrid spin-wave computing systems.

## SUPPLEMENTARY MATERIAL

See the [supplementary material](#) for methods, supplementary Figs. S1–S4, and supplementary movies S1–S12.

## ACKNOWLEDGMENTS

R.F.L.E. acknowledges computational resources from the VIKING cluster provided by the University of York. E.J.G.S. acknowledges computational resources through CIRRUS Tier-2 HPC Service (ec131 Cirrus Project) CIRRUS@EPCC (<http://www.cirrus.ac.uk>) funded by the University of Edinburgh and EPSRC (No. EP/P020267/1); and ARCHER UK National Supercomputing Service (<http://www.archer.ac.uk>) via Project d429. E.J.G.S. acknowledges the EPSRC Early Career Fellowship (No. EP/T021578/1) and the University of Edinburgh for funding support. K.S.N. acknowledges support by the Ministry of Education (Singapore) through the Research Centre of Excellence program (Award EDUN C-33-18-279-V12, Institute for Functional Intelligent Materials) and The Royal Society, UK.

## AUTHOR DECLARATIONS

### Conflict of Interest

The authors declare no conflict of interest.

## DATA AVAILABILITY

The data that support the findings of this study are available within the article and its [supplementary material](#).

## REFERENCES

- 1G. S. D. Beach, M. Tsoi, and J. L. Erskine, “Current-induced domain wall motion,” *J. Magn. Magn. Mater.* **320**, 1272–1281 (2008).
- 2G. Tatara, H. Kohno, and J. Shibata, “Microscopic approach to current-driven domain wall dynamics,” *Phys. Rep.* **468**, 213–301 (2008).
- 3D. Ralph and M. Stiles, “Spin transfer torques,” *J. Magn. Magn. Mater.* **320**, 1190–1216 (2008).
- 4S. S. P. Parkin, M. Hayashi, and L. Thomas, “Magnetic domain-wall racetrack memory,” *Science* **320**, 190–194 (2008).
- 5B. Huang *et al.*, “Layer-dependent ferromagnetism in a van der Waals crystal down to the monolayer limit,” *Nature* **546**, 270 (2017).
- 6C. Gong *et al.*, “Discovery of intrinsic ferromagnetism in two-dimensional van der Waals crystals,” *Nature* **546**, 265–269 (2017).
- 7Z. Guguchia *et al.*, “Magnetism in semiconducting molybdenum dichalcogenides,” *Sci. Adv.* **4**, eaat3672 (2018).
- 8D. R. Klein *et al.*, “Probing magnetism in 2D van der Waals crystalline insulators via electron tunneling,” *Science* **360**, 1218–1222 (2018).
- 9D. A. Allwood *et al.*, “Magnetic domain-wall logic,” *Science* **309**, 1688–1692 (2005).
- 10Z. Luo *et al.*, “Current-driven magnetic domain-wall logic,” *Nature* **579**, 214–218 (2020).
- 11P. Xu *et al.*, “An all-metallic logic gate based on current-driven domain wall motion,” *Nat. Nanotechnol.* **3**, 97–100 (2008).
- 12S.-H. Yang, K.-S. Ryu, and S. Parkin, “Domain-wall velocities of up to 750 m s<sup>-1</sup> driven by exchange-coupling torque in synthetic antiferromagnets,” *Nat. Nanotechnol.* **10**, 221–226 (2015).

- <sup>13</sup>S. Woo *et al.*, “Observation of room-temperature magnetic skyrmions and their current-driven dynamics in ultrathin metallic ferromagnets,” *Nat. Mater.* **15**, 501–506 (2016).
- <sup>14</sup>S. Vélez *et al.*, “High-speed domain wall racetracks in a magnetic insulator,” *Nat. Commun.* **10**, 4750 (2019).
- <sup>15</sup>S. A. Siddiqui, J. Han, J. T. Finley, C. A. Ross, and L. Liu, “Current-induced domain wall motion in a compensated ferrimagnet,” *Phys. Rev. Lett.* **121**, 057701 (2018).
- <sup>16</sup>K.-S. Ryu, L. Thomas, S.-H. Yang, and S. Parkin, “Chiral spin torque at magnetic domain walls,” *Nat. Nanotechnol.* **8**, 527–533 (2013).
- <sup>17</sup>M. Rabinovich and D. Trubetskov, *Oscillations and Waves: in Linear and Nonlinear Systems, Mathematics and its Applications* (Springer Netherlands, 2011).
- <sup>18</sup>S. Parkin and S.-H. Yang, “Memory on the racetrack,” *Nat. Nanotechnol.* **10**, 195–198 (2015).
- <sup>19</sup>V. Baltz *et al.*, “Antiferromagnetic spintronics,” *Rev. Mod. Phys.* **90**, 015005 (2018).
- <sup>20</sup>R. P. Cowburn and M. E. Welland, “Room temperature magnetic quantum cellular automata,” *Science* **287**, 1466–1468 (2000).
- <sup>21</sup>D. A. Allwood *et al.*, “Submicrometer ferromagnetic NOT gate and shift register,” *Science* **296**, 2003–2006 (2002).
- <sup>22</sup>M. Diegel, S. Glathe, R. Mattheis, M. Scherzinger, and E. Halder, “A new four bit magnetic domain wall based multibit counter,” *IEEE Trans. Magn.* **45**, 3792–3795 (2009).
- <sup>23</sup>H. H. Kim *et al.*, “One million percent tunnel magnetoresistance in a magnetic van der Waals heterostructure,” *Nano Lett.* **18**, 4885–4890 (2018).
- <sup>24</sup>D. Ghazaryan *et al.*, “Magnon-assisted tunnelling in van der Waals heterostructures based on CrBr<sub>3</sub>,” *Nat. Electron.* **1**, 344–349 (2018).
- <sup>25</sup>F. Cantos-Prieto *et al.*, “Layer-dependent mechanical properties and enhanced plasticity in the van der Waals chromium trihalide magnets,” *Nano Lett.* **21**, 3379–3385 (2021).
- <sup>26</sup>C. Chappert, A. Fert, and F. N. Van Dau, “The emergence of spin electronics in data storage,” *Nat. Mater.* **6**, 813–823 (2007).
- <sup>27</sup>A. Manchon *et al.*, “Current-induced spin-orbit torques in ferromagnetic and antiferromagnetic systems,” *Rev. Mod. Phys.* **91**, 035004 (2019).
- <sup>28</sup>V. Gupta *et al.*, “Manipulation of the van der Waals magnet Cr<sub>2</sub>Ge<sub>2</sub>Te<sub>6</sub> by spin-orbit torques,” *Nano Lett.* **20**, 7482–7488 (2020).
- <sup>29</sup>X. Wang *et al.*, “Current-driven magnetization switching in a van der Waals ferromagnet Fe<sub>3</sub>GeTe<sub>2</sub>,” *Sci. Adv.* **5**, eaaw8904 (2019).
- <sup>30</sup>D. A. Wahab *et al.*, “Quantum rescaling, domain metastability, and hybrid domain-walls in 2D CrI<sub>3</sub> magnets,” *Adv. Mater.* **33**, 2004138 (2021).
- <sup>31</sup>Q.-C. Sun *et al.*, “Magnetic domains and domain wall pinning in atomically thin CrBr<sub>3</sub> revealed by nanoscale imaging,” *Nat. Commun.* **12**, 1989 (2021).
- <sup>32</sup>A. Kartsev, M. Augustin, R. F. L. Evans, K. S. Novoselov, and E. J. G. Santos, “Biquadratic exchange interactions in two-dimensional magnets,” *npj Comput. Mater.* **6**, 150 (2020).
- <sup>33</sup>D. Soriano, M. I. Katsnelson, and J. Fernández-Rossier, “Magnetic two-dimensional chromium trihalides: A theoretical perspective,” *Nano Lett.* **20**, 6225–6234 (2020).
- <sup>34</sup>L. Chen *et al.*, “Topological spin excitations in honeycomb ferromagnet CrI<sub>3</sub>,” *Phys. Rev. X* **8**, 041028 (2018).
- <sup>35</sup>A. R. Wildes, M. E. Zhitomirsky, T. Ziman, D. Lançon, and H. C. Walker, “Evidence for biquadratic exchange in the quasi-two-dimensional antiferromagnet FePS<sub>3</sub>,” *J. Appl. Phys.* **127**, 223903 (2020).
- <sup>36</sup>M. Augustin, S. Jenkins, R. F. L. Evans, K. S. Novoselov, and E. J. G. Santos, “Properties and dynamics of meron topological spin textures in the two-dimensional magnet CrCl<sub>3</sub>,” *Nat. Commun.* **12**, 185 (2021).
- <sup>37</sup>L. N. Kapoor *et al.*, “Observation of standing spin waves in a van der Waals magnetic material,” *Adv. Mater.* **33**, 2005105 (2021).
- <sup>38</sup>M. Abramchuk *et al.*, “Controlling magnetic and optical properties of the van der Waals crystal CrCl<sub>3-x</sub>Br<sub>x</sub> via mixed halide chemistry,” *Adv. Mater.* **30**, 1801325 (2018).
- <sup>39</sup>S. Jiang, L. Li, Z. Wang, K. F. Mak, and J. Shan, “Controlling magnetism in 2D CrI<sub>3</sub> by electrostatic doping,” *Nat. Nanotechnol.* **13**, 549–553 (2018).
- <sup>40</sup>H. H. Kim *et al.*, “Evolution of interlayer and intralayer magnetism in three atomically thin chromium trihalides,” *Proc. Natl. Acad. Sci.* **116**, 11131–11136 (2019).
- <sup>41</sup>A. Hubert and R. Schafer, *Magnetic Domains: The Analysis of Magnetic Microstructures* (Springer Science and Business Media, 2008).
- <sup>42</sup>N. L. Schryer and L. R. Walker, “The motion of 180° domain walls in uniform dc magnetic fields,” *J. Appl. Phys.* **45**, 5406 (1974).
- <sup>43</sup>P. J. Metaxas *et al.*, “Creep and flow regimes of magnetic domain-wall motion in ultrathin Pt/Co/Pt films with perpendicular anisotropy,” *Phys. Rev. Lett.* **99**, 217208 (2007).
- <sup>44</sup>S. Pizzini *et al.*, “Chirality-induced asymmetric magnetic nucleation in Pt/Co/AlO<sub>x</sub> ultrathin microstructures,” *Phys. Rev. Lett.* **113**, 047203 (2014).
- <sup>45</sup>M. Bode, “Spin-polarized scanning tunnelling microscopy,” *Rep. Prog. Phys.* **66**, 523–582 (2003).
- <sup>46</sup>F. Casola, T. van der Sar, and A. Yacoby, “Probing condensed matter physics with magnetometry based on nitrogen-vacancy centres in diamond,” *Nat. Rev. Mater.* **3**, 17088 (2018).
- <sup>47</sup>M. Yamanouchi, D. Chiba, F. Matsukura, T. Dietl, and H. Ohno, “Velocity of domain-wall motion induced by electrical current in the ferromagnetic semiconductor (Ga,Mn)As,” *Phys. Rev. Lett.* **96**, 096601 (2006).
- <sup>48</sup>I. M. Miron *et al.*, “Fast current-induced domain-wall motion controlled by the Rashba effect,” *Nat. Mater.* **10**, 419–423 (2011).
- <sup>49</sup>S. Emori, U. Bauer, S.-M. Ahn, E. Martinez, and G. S. D. Beach, “Current-driven dynamics of chiral ferromagnetic domain walls,” *Nat. Mater.* **12**, 611–616 (2013).
- <sup>50</sup>R. Wieser, E. Y. Vedmedenko, and R. Wiesendanger, “Domain wall motion damped by the emission of spin waves,” *Phys. Rev. B* **81**, 024405 (2010).
- <sup>51</sup>S. Zhang and Z. Li, “Roles of nonequilibrium conduction electrons on the magnetization dynamics of ferromagnets,” *Phys. Rev. Lett.* **93**, 127204 (2004).
- <sup>52</sup>A. Thiaville, Y. Nakatani, J. Miltat, and Y. Suzuki, “Micromagnetic understanding of current-driven domain wall motion in patterned nanowires,” *Europhys. Lett.* **69**, 990–996 (2005).
- <sup>53</sup>M. Hayashi *et al.*, “Influence of current on field-driven domain wall motion in permalloy nanowires from time resolved measurements of anisotropic magnetoresistance,” *Phys. Rev. Lett.* **96**, 197207 (2006).
- <sup>54</sup>X. S. Wang and X. R. Wang, “Spin wave emission in field-driven domain wall motion,” *Phys. Rev. B* **90**, 184415 (2014).
- <sup>55</sup>P. Lederer and D. L. Mills, “Possible experimental test of the band theory of magnetism,” *Phys. Rev.* **148**, 542–547 (1966).
- <sup>56</sup>V. Vlaminck and M. Bailleul, “Current-induced spin-wave Doppler shift,” *Science* **322**, 410–413 (2008).
- <sup>57</sup>M. Zhu, C. L. Dennis, and R. D. McMichael, “Temperature dependence of magnetization drift velocity and current polarization in Ni<sub>80</sub>Fe<sub>20</sub> by spin-wave Doppler measurements,” *Phys. Rev. B* **81**, 140407 (2010).
- <sup>58</sup>K. Sekiguchi *et al.*, “Time-domain measurement of current-induced spin wave dynamics,” *Phys. Rev. Lett.* **108**, 017203 (2012).
- <sup>59</sup>G. B. Whitham, *Linear and Nonlinear Waves* (John Wiley & Sons Inc., 1974).
- <sup>60</sup>F. Bonnefoy *et al.*, “From modulational instability to focusing dam breaks in water waves,” *Phys. Rev. Fluids* **5**, 034802 (2020).
- <sup>61</sup>G. Marcucci *et al.*, “Topological control of extreme waves,” *Nat. Commun.* **10**, 5090 (2019).
- <sup>62</sup>P. G. Kevrekidis, D. J. Frantzeskakis, and R. Carretero-González, *The Defocusing Nonlinear Schrödinger Equation* (SIAM, Philadelphia, 2015).
- <sup>63</sup>S. M. Mohseni *et al.*, “Spin torque generated magnetic droplet solitons,” *Science* **339**, 1295–1298 (2013).
- <sup>64</sup>E. Iacocca *et al.*, “Spin-current-mediated rapid magnon localization and coalescence after ultrafast optical pumping of ferrimagnetic alloys,” *Nat. Commun.* **10**, 1756 (2019).
- <sup>65</sup>E. Iacocca, T. J. Silva, and M. A. Hofer, “Breaking of Galilean invariance in the hydrodynamic formulation of ferromagnetic thin films,” *Phys. Rev. Lett.* **118**, 017203 (2017).
- <sup>66</sup>S. K. Ivanov, A. M. Kamchatnov, T. Congy, and N. Pavloff, “Solution of the Riemann problem for polarization waves in a two-component Bose-Einstein condensate,” *Phys. Rev. E* **96**, 062202 (2017).
- <sup>67</sup>A. Gelash *et al.*, “Bound state soliton gas dynamics underlying the spontaneous modulational instability,” *Phys. Rev. Lett.* **123**, 234102 (2019).
- <sup>68</sup>L. J. Cornelissen, J. Liu, R. A. Duine, J. B. Youssef, and B. J. van Wees, “Long-distance transport of magnon spin information in a magnetic insulator at room temperature,” *Nat. Phys.* **11**, 1022–1026 (2015).

- <sup>69</sup>C. Liu *et al.*, “Long-distance propagation of short-wavelength spin waves,” *Nat. Commun.* **9**, 738 (2018).
- <sup>70</sup>Y. Kajiwara *et al.*, “Transmission of electrical signals by spin-wave interconversion in a magnetic insulator,” *Nature* **464**, 262–266 (2010).
- <sup>71</sup>W. Xing *et al.*, “Magnon transport in quasi-two-dimensional van der Waals antiferromagnets,” *Phys. Rev. X* **9**, 0111026 (2019).
- <sup>72</sup>A. Bedoya-Pinto *et al.*, “Intrinsic 2D-XY ferromagnetism in a van der Waals monolayer,” *Science* **374**(6567), 616–620 (2021).
- <sup>73</sup>S. Kezilebieke *et al.*, “Electronic and magnetic characterization of epitaxial CrBr<sub>3</sub> monolayers on a superconducting substrate,” *Adv. Mater.* **33**, 2006850 (2021).
- <sup>74</sup>H. Wang, F. Fan, S. Zhu, and H. Wu, “Doping enhanced ferromagnetism and induced half-metallicity in CrI<sub>3</sub> monolayer,” *Europhys. Lett.* **114**, 47001 (2016).
- <sup>75</sup>S. Zhang and S. S.-L. Zhang, “Generalization of the Landau-Lifshitz-Gilbert equation for conducting ferromagnets,” *Phys. Rev. Lett.* **102**, 086601 (2009).
- <sup>76</sup>K.-W. Kim, J.-H. Moon, K.-J. Lee, and H.-W. Lee, “Prediction of giant spin motive force due to Rashba spin-orbit coupling,” *Phys. Rev. Lett.* **108**, 217202 (2012).
- <sup>77</sup>M. D. Petrović, U. Bajpai, P. Plecháč, and B. K. Nikolić, “Annihilation of topological solitons in magnetism with spin-wave burst finale: Role of nonequilibrium electrons causing nonlocal damping and spin pumping over ultrabroadband frequency range,” *Phys. Rev. B* **104**, L020407 (2021).
- <sup>78</sup>T. Weindler *et al.*, “Magnetic damping: Domain wall dynamics versus local ferromagnetic resonance,” *Phys. Rev. Lett.* **113**, 237204 (2014).
- <sup>79</sup>S. S. Dhillon *et al.*, “The 2017 terahertz science and technology roadmap,” *J. Phys. D* **50**, 043001 (2017).